Design, construction, and testing of a parabolic trough solar concentratorfor hot water and low enthalpy steam generation

Article *in* Journal of Renewable and Sustainable Energy · September 2012

DOI: 10.1063/1.4751461

CITATIONS
84

READS
7,194

5 authors, including:

Eduardo Venegas
Mexican Institute of Water Technology (IMTA)
32 PUBLICATIONS **360** CITATIONS
SEE PROFILE

O.A. Jaramillo
National Autonomous University of Mexico
67 PUBLICATIONS **2,382** CITATIONS
SEE PROFILE

J. O. Aguilar
University of Quintana Roo
32 PUBLICATIONS **936** CITATIONS
SEE PROFILE

AIP | Journal of Renewable and Sustainable Energy

Design, construction, and testing of a parabolic trough solar concentrator for hot water and low enthalpy steam generation

E. Venegas-Reyes, O. A. Jaramillo, R. Castrejón-García, J. O. Aguilar, and F. Sosa-Montemayor

Citation: J. Renewable Sustainable Energy **4**, 053103 (2012); doi: 10.1063/1.4751461
View online: http://dx.doi.org/10.1063/1.4751461
View Table of Contents: http://jrse.aip.org/resource/1/JRSEBH/v4/i5
Published by the American Institute of Physics.

Design, construction, and testing of a parabolic trough solar concentrator for hot water and low enthalpy steam generation

E. Venegas-Reyes,[1] O. A. Jaramillo,[2,a)] R. Castrejón-García,[2]
J. O. Aguilar,[3] and F. Sosa-Montemayor[1]
[1]*Posgrado en Ingeniería, Universidad Nacional Autónoma de México, Privada Xochicalco s/n, Temixco, Morelos 62580, Mexico*
[2]*Centro de Investigación en Energía, Universidad Nacional Autónoma de México, Privada Xochicalco s/n, Temixco, Morelos 62580, Mexico*
[3]*Universidad de Quintana Roo, Boulevard Bahía s/n, Quintana Roo 77019, Mexico*

(Received 6 March 2012; accepted 24 August 2012; published online 12 September 2012)

This paper reports the design, construction, and evaluation of a solar parabolic trough concentrator (PTC) with a rim angle of 45°, a length of 4.88 m, and an aperture area of 5.8 m^2. The PTC is made of aluminium in such a way that both the manufacturing and assembly processes do not require complicated technology or skilled labour. Since the PTC is for low enthalpy steam generation and hot water, it is designed with an unshielded receiver and without a glass cover in order to reduce both production and transportation costs. A finite element stress analysis is conducted to determine the mechanical behaviour of the PTC under various simulated wind loads on the structure. A simple solar tracking system is employed when it is oriented in a North-to-South direction. The optical efficiency of the collector is also reported. Said efficiency depends on the optical properties of the materials involved, the geometry of the collector, and the various imperfections arising from the construction of the collector. The thermal performance of the PTC was determined according to the Standard ASHRAE 93-1986 (RA 91). Peak efficiencies close to 60% were obtained. © *2012 American Institute of Physics*. [http://dx.doi.org/10.1063/1.4751461]

I. INTRODUCTION

At low and medium temperatures, solar heat can be used in industries involved in chemical, paper, textiles, and food preparation, in processes such as drying, sterilizing, cleaning, evaporating, steaming, and conditioning (heating and cooling) of industrial buildings. Hot water or low-pressure steam at medium temperatures (80-250°) can be used either for pre-heating water (or other fluids), for household processes (washing, dyeing, etc.), for steam generation, or, by direct coupling of the solar system, for individual process in which working temperatures are lower than that of the central steam supply.

In recent years, research on solar heating for industrial processes has addressed the development of new devices, new applications, control methodologies, thermodynamic and technical-economic analysis, as well as the development of components, support structures, reflective materials, materials for the receiver, and absorber surfaces. In the literature, there exist diverse methodologies for the design and optimization of the integration of these systems to industrial processes,[1–4] some of them successful;[5] there are also solar cooling and refrigeration processes,[6,7] including hybrid thermal-photovoltaic ones.[8] For medium temperature processes, the food industry has great potential. This is particularly important for developing

a)Author to whom correspondence should be addressed. Electronic mail: ojs@cie.unam.mx. Fax: +52 (777) 325 0018.

TABLE I. Thermal efficiency for different types of PTCs.

Equation	Reference
$\eta_I = 0.66 - 0.233(\Delta T/G_b)$	10
$\eta_I = 0.65 - 0.382(\Delta T/G_b)$	11
$\eta_I = 0.642 - 0.441(\Delta T/G_b)$	12
$\eta_I = 0.638 - 0.387(\Delta T/G_b)$	13
$\eta_I = 0.69 - 0.39(\Delta T/G_b)$	14 and 15
$\eta_I = 0.0543 - 0.1889(\Delta T/G_b)$	16

countries, where improvement and modernization of the food industry play a critical role in terms of food security. It is important to note that solar heat for industrial processes can help to stabilize food prices by reducing their dependence on the volatility of oil prices and other energy sources.[9]

Some industrial processes can be driven by medium-temperature parabolic trough concentrators (PTCs). For instance, there are different designs of PTCs for the production of hot water and low enthalpy steam. These concentrators are modular, with solar collection areas in the range of 2.5 to 5.0 m^2. Table I shows the efficiency curves that have been reported in the literature for this type of PTC.

Soil disinfestation by hot water and steam is an agricultural technique that has recently been attracting growing interest due to its low ecological impact, in particular, where operating temperatures are in the range of 70 to 110 °C.[17–20] This process represents a viable alternative to the use of methyl bromide, which will soon be banned in many countries. Methyl bromide is readily photolyzed in the atmosphere and released as elemental bromine, which is far more destructive to stratospheric ozone than chlorine. As such, it is subject to phase-out requirements of the 1987 Montreal Protocol on Ozone Depleting Substances. The aim of this paper is to develop a solar technology to provide low enthalpy steam and hot water in the range of 70 to 110 °C that can be applied to soil disinfection. It is clear that the PTC technology is widely studied in literature. However, we considered that one of the main contributions of this paper is the design and construction of a solar concentrator that is inexpensive and easy to manufacture while still being able to deliver industrial quality steam and hot water; additionally, we present straightforward procedures for calculating the theoretical thermal behaviour and for estimating the contour error that relates to the optical efficiency of the PTC.

In this work, we present the design, construction, and optical and thermal evaluation of a PTC with a rim angle of 45°, a length of 4.88 m, and an aperture area of 5.8 m^2. The PTC uses water as working fluid; it was found to reach peak efficiencies close to 60% with a flow rate of 6 lpm at a direct solar irradiance of 865 W/m^2 with incidence angle of 0°. The results show that the PTC provides an adequate thermal efficiency and enough structural resistance. Because of its modular design, several PTCs can be connected in series, providing an increment in the thermodynamic availability of the fluid.

The paper is organized as follows. In Sec. II, we present the design and construction of the PTC. In this section, we report the dimensions and parameters of the collector, a finite element stress analysis and a description of the collector tracking system. In Sec. III, we report the optical behaviour of the PTC by considering both the optical efficiency and the intercept factor. A method to estimate the random optical error of the PTC is also reported. In Sec. IV, we describe a theoretical model used to compute the thermal efficiency of the PTC. In Sec. V, we describe the evaluation of the thermal performance of the PTC established by the thermal efficiency for different flow rates according to the Standard ASHRAE 93-1986 (RA 91). The heat removal factor and the total heat loss coefficient of the PTC are included in this section. In Sec. VI, we report the actual initial cost of the described solar PTC system. The main findings and results of the research are presented in Sec. VII.

II. DESIGN AND CONSTRUCTION

The PTC, we present here, has the following innovative characteristics: low cost of manufacturing materials, light and strong structure, and easy construction. In order to reduce construction expenses, two commercially available "off-the-shelf" aluminium foils (1.22 m by 2.44 m) were used. They were placed longitudinally; this in turn determined the size of the PTC. We chose an aluminium foils developed by Alanod 4270AG,[21] since it reflects 95% of sunlight. As part of the design of the PTC, the aluminium foils are not cut or rolled; the aluminium foils are installed on the structure without modification, the parabolic profile is given by the shape of the ribs and the weight of the foils as they rest on said ribs.

A. Parameters of the PTC

In order to determine the dimensions of the PTC, we considered the following parameters: a rim angle of 45° ($\varphi_r = 45°$) and the width of the aluminium foil $S = 1.22$ m. Based on these two parameters, it is possible to determine the aperture of the parabola, W_a,[31]

$$W_a = \frac{2S\tan\left(\frac{\varphi_r}{2}\right)}{\left(\sec\left(\frac{\varphi_r}{2}\right)\tan\left(\frac{\varphi_r}{2}\right) + \ln\left(\sec\left(\frac{\varphi_r}{2}\right) + \tan\left(\frac{\varphi_r}{2}\right)\right)\right)} \tag{1}$$

and the focal length, f,[31]

$$f = \frac{W_a}{4\tan\left(\frac{\varphi_r}{2}\right)}. \tag{2}$$

On the other hand, the geometric concentration ratio, C is given by[31]

$$C = \frac{W_a}{\pi D_o}, \tag{3}$$

where W_a is the width of the collector and D_o is the outer diameter of the receiver. For the manufacture of the receiver, a commercial copper tube with outer diameter of 1 inch ($D_o = 2.54$ cm) is used. It is important to point out that the surface of the receiver tube was painted with Zynolyte, a well-characterized coating.[22] This paint has an absorptance $\alpha = 0.95$. Table II gives a summary of the PTC key features.

It can be shown that, for different rim angles, the focus-to-aperture ratio, which defines the curvature of the parabola, changes. It can be demonstrated that, with a 90° rim angle, the mean focus-to-reflector distance and hence the reflected beam spread is minimized, so that the slope and tracking errors are less pronounced.[31] It is important to point out that using a commercial "off-the-shelf" sheet with a width of 1.22 m and a rim angle of 90° would results in an aperture W_a of 1.063 m (Eq. (1)) and a concentration ratio of 13.3 (Eq. (3)). On the other hand, if the rim angle is 45°, an aperture of 1.187 m and a concentration ratio of 14.9 are obtained.

TABLE II. PTC key features.

	Collector parameters
φ_r (°)	45°
f (m)	0.716
W_a (m)	1.187
D_o (m)	0.0254
L (m)	$2 \times 2.44 = 4.88$
A_a (m^2)	5.793
C (-)	14.87

Therefore, the sacrifice in optical efficiency is small, while the increment in concentration ratio and aperture area is significant. This allows savings in reflective materials cost.

In Subsection II B, we describe the structural analysis performed to the PTC with the idea of estimating the mechanical behaviour when it is subjected to different mechanical stresses.

B. Construction and structural analysis

The PTC is constructed in a simple manner; it comprises 7 aluminium ribs, 5 aluminium tubes, and a rectangular hollow section (RHS) as the main structure. The ribs were joined by using five aluminium tubes with an outer diameter of 35.5 mm, each joint is completed by using setscrews. The RHS is made of steel to provide a strong backbone to the PTC. This element prevents passive flexion deformity due to its own weight. Fig. 1 shows the basic structure of the collector. Furthermore, to hold the aluminium foils onto the structure of the PTC, a rectangular frame made of aluminium is used. This frame is then screwed at the ends of each rib.

The seven ribs were cut with the parabolic profile and they made from an aluminium plate with a thickness of 10 mm. These elements are the most expensive components of the PTC because they were constructed by using a computer numerical control (CNC), which ensures high accuracy in the geometry and correct dimensions of the profile. The rest of the structural parts (hollow rectangular section, aluminium profiles, and tubes) are commercial and only require very simple machining (drilling and cutting) in order to be properly fitted. In the construction of the PTC, there is no need for sophisticated machinery or skilled labour; and during the assembly, only hand tools are required. As can be seen in Figure 1, the structure is assembled using only screws and set screws. With the exception of the hollow rectangular section made of steel, all other elements are made of aluminium with the aim of having a light but robust structure that has good resistance to outdoor conditions.

Fig. 2 shows a picture of the PTC. Note that the receiver tube is supported by an O-ring of black nylamid polyamide (Nylon) in order to reduce the thermal contact between the receiver and the body of the structure (see Fig. 2). The thermal conductivity of the black nylamid is close to $k_N = 0.3\ W/m{\cdot}K$ with adequate thermal and mechanical properties.

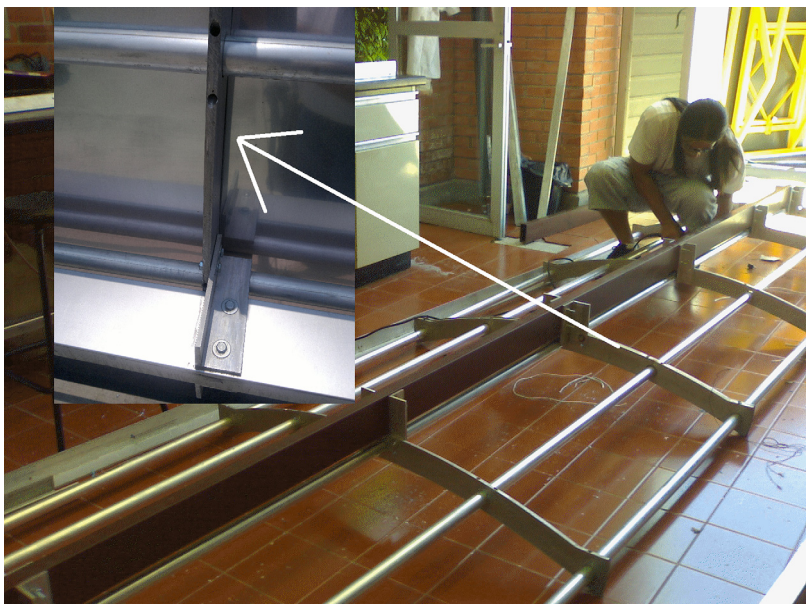

FIG. 1. Structure of the PTC and detail of its construction.

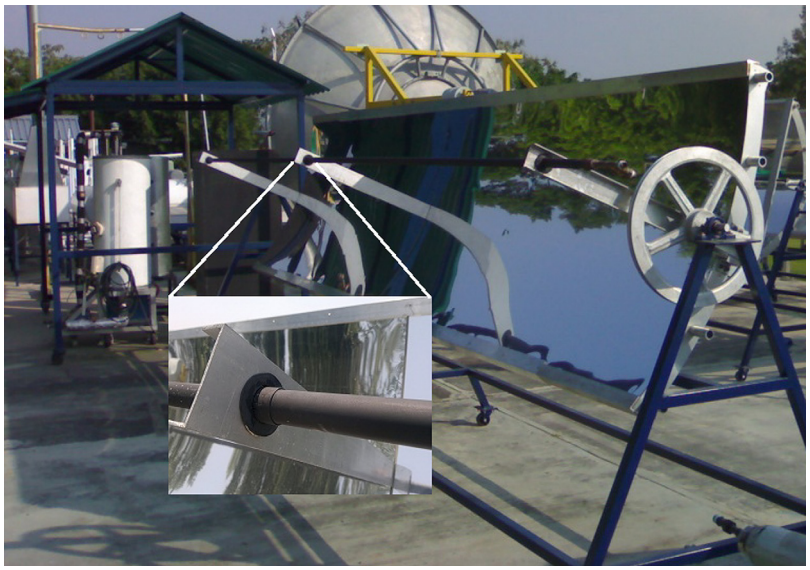

FIG. 2. Parabolic trough concentrator and receiver support.

In order to achieve an adequate thermodynamic availability, several collectors can be connected in series, allowing a rise in the temperature of the fluid flowing along the receiver tube. The use of properly insulated flexible pipes should be considered when interconnecting two or more collectors in series.

On the other hand, a finite element stress analysis is conducted to determine the mechanical behaviour of the PTC. In order to test the structural integrity of the design, different wind loads were simulated. It is important to point out that this analysis only discusses the structural resistance to static loads. The first analysis consisted in applying four loads of 200 N in the collector corners in such a way that the structure is subjected to torsion. In the second analysis, four lateral loads were applied, two loads of 200 N in outer ribs and two loads of 300 N in the internals ribs. A third case was performed by applying four loads of 300 N each one. They were applied in the normal direction to the collector aperture area, causing the collector to spread.

All of the previous simulations where done in the finite element analysis program called ALGOR.[23] Results are presented in Table III. They show that the most critical case is when the collector is subject to torsion loads. In this case, the minimum safety factor is 4.20 MPa, taking into account that the permissible stress of aluminium is 145 MPa, the structure of the PTC can resist these loads without permanent deformation. Due to the assembly of the ribs, the mechanical load applied to the front of the PTC showed the best results, with the lowest stress of 2.46 MPa and a deformation smaller than 0.32 mm. The maximum stress of 7.37 MPa occurs when the lateral load are applied with a maximum disablement close to 1.24 mm. Figure 3 shows a diagram of the loads applied in the PTC.

Subsection II C describes the sun tracking system developed in order to operate the PTC in a plane rotated about a horizontal east-west axis with continuous adjustment to minimize the angle of incidence.

TABLE III. FEA results for the PTC.

Analysis type	Loads (N)	Maximum stress (MPa)	Maximum displacements (mm)	Minimum safety factor
Torsion	200	7.07	0.38	4.20
Lateral	200 and 300	7.37	1.24	4.38
Frontal	200	2.46	0.32	12.57

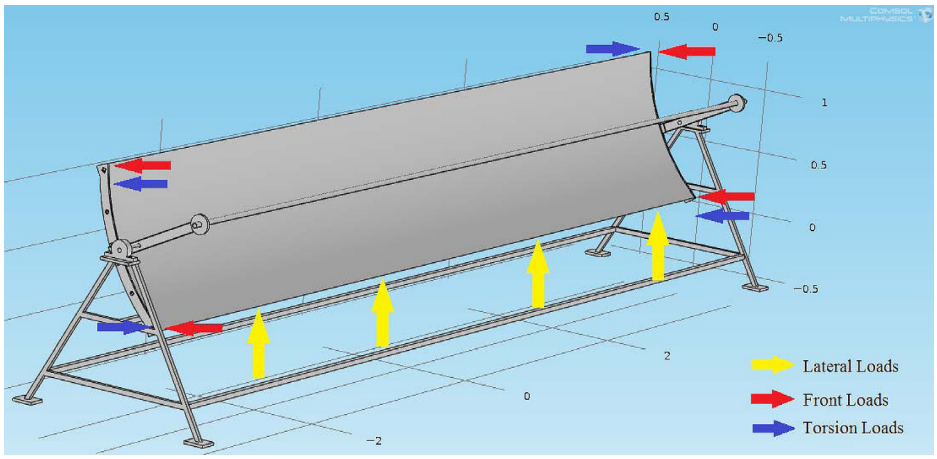

FIG. 3. Loads considered in the finite element stress analysis.

C. Sun tracking system

The sun tracking system is constituted by a DC-motor of 24 V with a power of 1/17 HP and a frequency of a rotation of 83.3 rpm. The DC-motor is coupled to a reduction of 30:1. The tracking system has two pulleys; one of them is coupled to the motor and the other one to a pulley with 20 inch (50.8 cm) in diameter that is coupled to the rotation shaft of the PTC. The pulleys are articulated by a flexible band in order to transmit the motor rotation.

On the other hand, the shaft of the DC-motor is coupled to a rotary encoder with a resolution of 2000 P/R, which calculates the angular displacement by using LABVIEW-based control interface. The CAD drawing of the tracking system is depicted in Fig. 4.

The LABVIEW interface is programmed to drive the DC-motor in discrete-time step. The hour angle is calculated and compared with the initial angular position of the collector. The time difference between the hour angle and the angular position of the aperture of the collector determines the displacement required from the DC-motor. For instance, the motor rotates when the difference between the hour angle and angular position is greater than 0.225° and when said difference is smaller than −0.225°, that is, a displacement of 0.45° every 1.8 min. Due to the size of the receiver tube, $D_o = 2.54$ cm, the solar tracking system may be driven by this discrete-time step, since the fraction of beam solar radiation that has been reflected by the parabola and consequently concentrates at the absorber tube during this period of time is equal to 1.

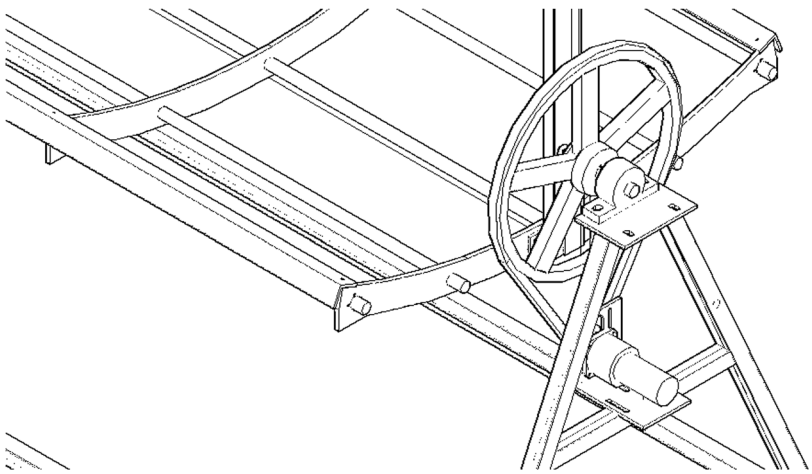

FIG. 4. Tracking system.

III. OPTICAL EFFICIENCY

The optical efficiency of a PTC, η_o, is the ratio of solar energy that falls on the surface of the absorber tube to that which falls on the reflective surface of the collector. It is commonly given as[31]

$$\eta_o = \lfloor \tau\alpha\,\rho\gamma(1 - A_f \tan\theta_i \cos\theta_i) \rfloor_n, \tag{4}$$

where ρ is the reflectance of the mirror surface, τ is the transmittance of the glass-shielded of the receiver (in our case, it is not taken into account, since an unshielded receiver was used), α is the absorptance of the receiver, γ is the intercept factor, A_f is the geometric factor, and θ_i is the angle of incidence. The subscript n indicates the evaluation of the parameters at the normal incidence of the solar beam radiation ($\theta_i = 0$), therefore, $\eta_o = [\tau\alpha\,\rho\gamma]_n$.

The parameter γ describes the interaction of all optical errors of the PTC and it is given by Güven and Bannerot,[24–26]

$$\gamma = \frac{1 + \cos(\varphi_r)}{2\sin(\varphi_r)} \int_0^{\varphi_r} \frac{\mathrm{erf}(M) - \mathrm{erf}(N)}{1 + \cos(\varphi)} d\varphi, \tag{5}$$

where

$$M = \frac{\sin(\varphi_r)\left(1 + \cos(\varphi)\right)\left(1 - 2d^*\sin(\varphi)\right) - \pi\beta^*\left(1 + \cos(\varphi_r)\right)}{\sqrt{2}\pi\sigma^*\left(1 + \cos(\varphi_r)\right)},$$

$$N = -\frac{\sin(\varphi_r)\left(1 + \cos(\varphi)\right)\left(1 + 2d^*\sin(\varphi)\right) + \pi\beta^*\left(1 + \cos(\varphi_r)\right)}{\sqrt{2}\pi\sigma^*\left(1 + \cos(\varphi_r)\right)},$$

φ is the angle between the parabolic axis and a point on mirror surface, φ_r is the rim angle, d_r is the receiver mislocation, $d^* = d_r/D$ the universal non-random error parameter due to receiver mislocation and D is the absorber tube diameter, $\beta^* = \beta C$ is the universal non-random error parameter due to angular errors and β is the tracking error angle, $\sigma^* = \sigma C$ is the universal random error parameter, σ is the random optical error, and C is the geometric concentration ratio.[25]

The standard deviation σ accounts for all optical errors and is given by the quadratic sum of individual errors[27]

$$\sigma = \sqrt{\sigma_{sun}^2 + 4\sigma_{contour}^2 + \sigma_{specular}^2}, \tag{6}$$

where σ_{sun} is the rms angular width of sun, $\sigma_{contour}$ the contour error, and $\sigma_{specular}$ is the error due to lack of perfect specularity.

In order to determine $\sigma_{contour}$, we start analysing the tangent of the parabola

$$\frac{dy}{dx} = \frac{x}{2f}, \tag{7}$$

where we substitute $f = x^2/4y$ in Eq. (7) to obtain

$$\frac{dy}{dx} = 2\frac{y}{x}. \tag{8}$$

Furthermore, the angle of the tangent at any point in the parabola is given by the following expression:

$$\tan\theta_t = 2\frac{y}{x}. \tag{9}$$

In this way, in order to establish the variance between the analytical and measured quantities, we can establish the following relationship:

$$|\Delta\theta_{t,i}| = \left|\arctan\left(2\frac{y_i}{x_i}\right) - \arctan\left(2\frac{y_i + \delta y_i}{x_i + \delta x_i}\right)_{med}\right|, \tag{10}$$

where $|\Delta\theta_{t,i}|$[rad] is the absolute value of the i-esimal measured variance, δx and δy are the difference between the analytical values and the measured data in the (x,y) plane.

In order to determine $\sigma_{contour}$, we compute the standard deviation of the error distribution, so that

$$\sigma_{contour} = \sqrt{\frac{1}{n}\left[\sum_{i=1}^{n}\left(|\Delta\theta_{t,i}| - \frac{\sum|\Delta\theta_{t,i}|}{n}\right)^2\right]}, \tag{11}$$

which is considered a Gaussian distribution of random errors.

In order to evaluate the errors of the parabolic surface of the PTC, a SOLO® portable coordinate measurement system[28] was used. This system consists of a computer, a plastic pole with several infrared light-emitters on its body (the probe), and an infrared CCD camera which senses the light of the infrared emitters. The camera acquires the spatial position of each light emitter and, based on this information, a computer code calculates the coordinates of the position (x, y, z) where the tip of the probe is placed. To calculate the deviation errors of a given surface, the computer code compares the coordinates of the tip with the coordinates of a CAD drawing stored in memory.

To test the parabolic trough, the trough's surface was scanned with the tip of the probe over one hundred and eighty different points along a path whilst keeping the coordinate z constant. The coordinates (x, y) for each of these probed points were then computed. Those values represent the coordinates of the points over the parabolic surface where the tip of the probe was placed. The differences between the measured points and the CAD drawing data are reported by the system as (δx, δy). Note that values of the vertex must be excluded to avoid a division by zero in Eq. (10).

Figure 5 shows both the profile of the curve produced by the measured points over the surface of the trough and the parabola CAD drawing.

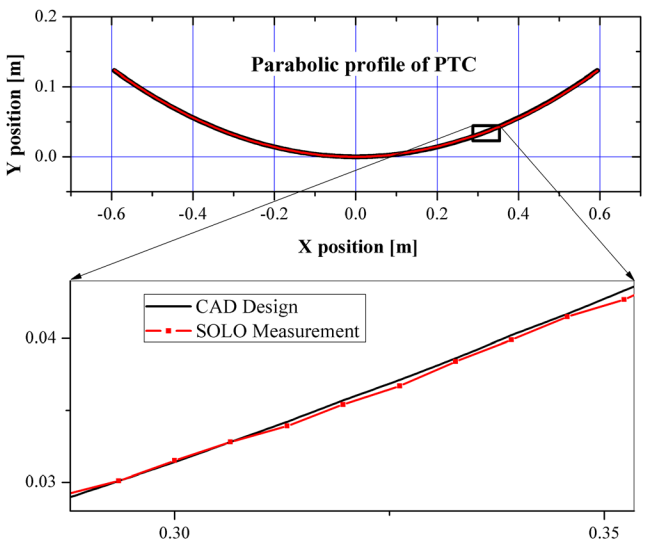

FIG. 5. Measured profile and parabola CAD drawing.

TABLE IV. Comparison of error parameters.

		Parameters given in Ref. 26		Reported in Ref. 29	This Work
Parameters	U. S. High-tech PTCs	Developing country		PTC 82°	PTC 45°
σ (rad)	0.0064	0.0087	0.0113	0.0113	0.0098
β (°)	0.25	0.50	1.00	0.375	0.50
d_r (mm)	3.10	6.20	6.20	7.75	7.50
D_o (mm)	24.8	24.8	24.8	30.00	25.4
C (-)	28.00	21.00	16.00	15.92	14.87
σ^* (rad)	0.1792	0.1827	0.1808	0.1798	0.1457
β^* (rad)	0.1222	0.1833	0.2793	0.1111	0.1298
d^* (-)	0.125	0.250	0.250	0.2583	0.2953

On the basis of the measured data, the value of the contour error is $\sigma_{contour} = 3.73 \times 10^{-3}$rad, and considering $\sigma_{sun} = 5.6 \times 10^{-3}$rad[27] and $\sigma_{specular} = 3.0 \times 10^{-3}$rad,[27] the random optical error is then

$$\sqrt{(5.6 \times 10^{-3})^2 + 4(3.73 \times 10^{-3})^2 + (3.0 \times 10^{-3})^2} = 0.0098.$$

Table IV reports the estimated values of the optical errors for the PTC and they are compared with those values reported in the literature.

Table V reports the optical efficiency η_o and intercept factor γ, both for an angle of incidence $\theta = 0$, (i.e., when the incidence of solar radiation is normal to the aperture area of the PTC).

In the next section we report a thermal model in order to estimate the performance of the PTC.

IV. THERMAL MODEL

The thermal analysis of a PTC without phase change is similar to that of a flat plate collector.[30,31] By doing an energy balance, the useful heat Q_u of the PTC is given by

$$Q_u = F_R \lfloor \eta_o A_a G_b - A_r U_L (T_{m,i} - T_a) \rfloor , \tag{12}$$

where F_R is the removal factor, η_o is the optical efficiency, A_a is the aperture area of the concentrator, G_b is the direct solar radiation, A_r is the receiver area, U_L is the coefficient of global losses, $T_{m,i}$ is the temperature at the entrance of the receiver, and T_a is the ambient temperature.

The instantaneous efficiency η is obtained from $Q_u/G_b A_a$, in the following way:[30,31]

$$\eta = F_R \eta_o - F_R \frac{U_L}{C} \left(\frac{T_{m,i} - T_a}{G_b} \right) . \tag{13}$$

TABLE V. Optical efficiency and intercept factor at normal incidence of the solar beam radiation.

Parameters	
η_o (-)	0.60
ρ (-)	0.95
τ (-)	—
α (-)	0.95
γ (-)	0.665

The removal factor F_R can be estimated in the following way:[30,31]

$$F_R = \frac{\dot{m}C_p}{A_r U_L}\left[1 - \exp\left(-\frac{U_L F' A_r}{\dot{m}C_p}\right)\right], \tag{14}$$

where $\dot{m}$ is the mass flow, C_P is the specific heat at constant pressure of the fluid, and the efficiency factor of the collector is calculated by[30,31]

$$F' = \frac{\frac{1}{U_L}}{\frac{1}{U_L} + \frac{D_o}{h_w D_i} + \left(\frac{D_o}{2k_w}\ln\left(\frac{D_o}{D_i}\right)\right)}, \tag{15}$$

where h_w and k_w are the fluids heat transference and thermal conductivity coefficients respectively, and D_o and D_i are the external and internal diameters of the receiver tube, respectively.

The value of k_w may be obtained from the literature[32] and the coefficient h_w can be calculated through the Nusselt number,

$$h_w = \frac{k_w Nu_D}{D_i}. \tag{16}$$

If it is turbulent flow (Re $>$ 2300), then

$$Nu_D = 0.023(\mathrm{Re})^{0.8}(\mathrm{Pr})^{0.4}, \tag{17}$$

where Pr is the Prandtl number and Re is the Reynolds number. If the flow is laminar (Re $\leq$ 2000), then Nu_D is a constant,[32]

$$Nu_D = 4.364. \tag{18}$$

In order to determine the flow regime, the fluid is considered as incompressible inside a transversal section of the collector tube; and in a permanent state, in this way, the Reynolds number is obtained by[32]

$$\mathrm{Re}_D = \frac{4\dot{m}}{\pi D_i \mu_w}, \tag{19}$$

where μ_w is the dynamic viscosity of the fluid.

On the other hand, in order to calculate U_L in the unshielded receiver, we assume that there are no important temperature gradients along the receiver. Taking into account the radiation and the convection on the external surface of the receiver tube, we have[31]

$$U_L = h_r + h_v, \tag{20}$$

where h_r is the radiative heat transfer coefficient, and h_v is the transfer coefficient due to wind-associated heat transfer. It is important to note that the conduction through the support structure is not taken into account because this is isolated as can be seen in Figure 2.

The linearization of the radiative heat transfer coefficient can be estimated by[31]

$$h_r = 4\sigma\varepsilon_r T_r^3, \tag{21}$$

where σ is the Stefan-Boltzmann constant, ε_r is the receiver's surface emissivity, and T_r is the surface temperature of the receiver.

In order to estimate the loss coefficient due to wind h_v, the Zhukauskas[32] relation is used

$$\overline{Nu_D} = (B)\,(\overline{\mathrm{Re}_D})^m(\mathrm{Pr})^n\left(\frac{\mathrm{Pr}}{\mathrm{Pr}_r}\right)^{1/4}, \quad \begin{bmatrix} 0.7 < \mathrm{Pr} < 500 \\ 1 < \mathrm{Re}_D < 10^6 \end{bmatrix}, \tag{22}$$

where $\overline{\mathrm{Re}_D}$ is the Reynolds number for a circular cylinder in crossflow defined as

$$\overline{\mathrm{Re}_D} = \frac{VD_o}{\nu}, \tag{23}$$

where V is the wind velocity and ν is the kinematic viscosity of the air.

Almost all of the variables in Eq. (22) are evaluated at ambient temperature T_a, the exception is Pr_r that depends on T_r. If $\mathrm{Pr} \leq 10$, then $n = 0.37$, however if $\mathrm{Pr} > 10$ then $n = 0.36$. The values of B and m are listed in Table VI.

In this way, the estimation of the coefficient of losses due to wind h_v is determined by the following relation:[32]

$$h_v = \overline{Nu_D}\,\frac{k_v}{D_o}, \tag{24}$$

where k_v is the thermal conductivity of air, and D_o is the external diameter of the receiver tube.

In order to estimate T_r, an energy balance is performed on the receiver tube where it is stipulated that the receiver has a high thermal diffusivity and also has thin walls (i.e., copper is used as the receiver tube's material, $\alpha = 117 \times 10^6$ [m^2/s]). Therefore, T_r is the same inside as well as outside the receiver's surface. Thus, we can write

$$h_w(T_r - T_{m,o}) = \eta_o C G_b, \tag{25}$$

where $T_{m,o}$ is the mean fluid temperature at the receiver's exit. In this way, the estimated value of T_r is

$$T_r = \frac{\eta_o C G_b}{h_w} + T_{m,o}, \tag{26}$$

where h_w is the work fluid's convective heat transference coefficient (Eq. (16)).

In order to determine $T_{m,o}$, an energy balance is developed in the following way:

$$\eta_o C G_b A_r = \dot{m} C_p (T_{m,o} - T_{m,i}), \tag{27}$$

where $T_{m,i}$ is the receiver tube's inlet temperature. When taking into account the receiver's area $A_r = \pi D_o L$, we can write

$$T_{m,o} = \frac{\eta_o C G_b (\pi D_o L)}{\dot{m} C_p} + T_{m,i}. \tag{28}$$

TABLE VI. Constants of the correlation due to Zhukauskas (Ref. 32).

$\overline{\mathrm{Re}_D}$	B	m
0.4–4	0.989	0.330
4–40	0.911	0.385
40–4000	0.683	0.466
4000–40 000	0.193	0.618
40 000–400 000	0.027	0.805

To evaluate the instantaneous efficiency η (Eq. (13)), we used the thermophysical properties of saturated water and air at atmospheric pressure reported in Ref. 32. The heat transfer fluid is circulated at 4 lpm to ensure turbulent conditions in the absorber and reasonable temperature rise for the expected levels of irradiance close to 865 W/m^2. Fig. 6 depicts the instantaneous efficiency for the theoretical model.

In Sec. V, we report the collector time constant, the thermal efficiency, and the incidence angle modifier for the PTC.

V. THERMAL PERFORMANCE

The PTC was evaluated according to the ASHRAE 93-1986 (RA 91) standard.[34] This standard is widely known and provides test methods for determining the thermal efficiency of a concentrating collector (section 8.2.1.1). The evaluation of the PTC was conducted to determine the time constant, the thermal efficiency, and the incidence angle modifier. It is important to note that during the evaluation process, the PTC was rotated about a horizontal east-west axis with an adjustment in the north-south plane in order to minimize the angle incidence. Therefore, the solar tracking system was not used to follow the sun.

A system was built to provide preheated water for the characterization of the PTC, and at the same time to act as heat storage. It is composed of a storage tank, an electrical water heating system (with automatic temperature control), and the hydraulic circuit. It can provide hot water with temperatures in the range from ambient up to 90 ± 1.0 °C.

Water in the storage tank is heated by electrical resistors of 3 and 6 kW. The temperature is regulated by the temperature control system, whose feedback is a thermocouple located in the tank (see Fig. 7). The preheated water is fed to the PTC by a ½ hp centrifugal pump. The flow rate can be controlled by a needle valve and is monitored by Headland series HB2800 flowmeter. Temperature and pressure are also monitored at the storage tank exit. The water can be recirculated to the storage tank in order to increase the heating speed and to get a more uniform temperature (by opening valve V7 and closing V9 and V10). Once the desired temperature is reached in the thermo tank, V9 and V10 are opened (the latter to allow fresh water at temperature ambient to enter to the tank) and V7 is closed. In order to measure the solar beam radiation, an Eppley pyrheliometer, mod. NIP, was used. The acquisition was completed by an Agilent Technologies 34970 A data acquisition system, with an HP34901A multiplexer card and a personal computer.

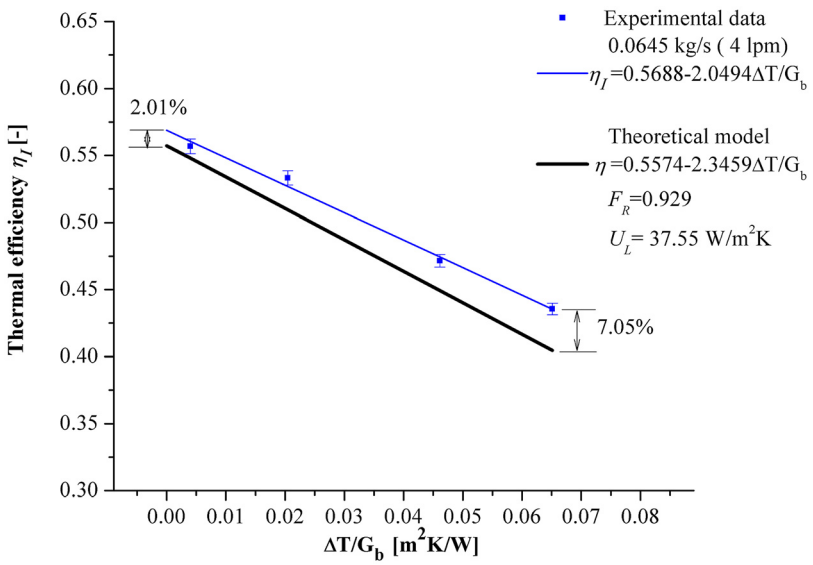

FIG. 6. Theoretical model for instantaneous efficiency.

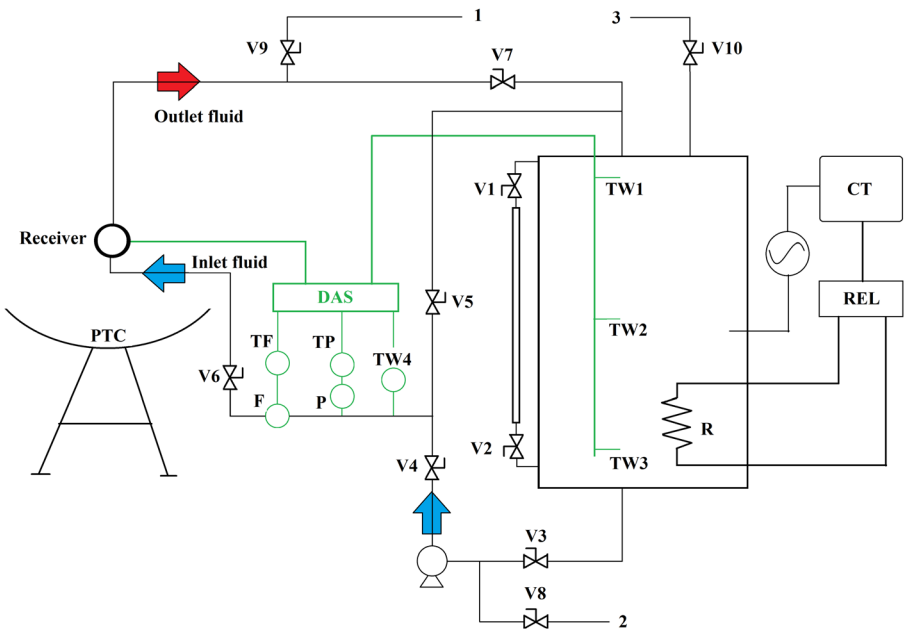

FIG. 7. Diagram of the experimental system.

A. Time constant

The time constant of the PTC was obtained by following the test suggested by the ASHRAE 93-1986 (RA 91) standard.[33] The time constant is established by solving

$$\frac{T_{o,t} - T_i}{T_{o,\text{int}} - T_i} = \frac{1}{e} = 0.368, \tag{29}$$

where T_i is the inlet temperature, $T_{o,t}$ is the outlet temperature at the time t, and $T_{o,\text{int}}$ is the temperature at the outlet when the beam radiation is obstructed for the cooling time constant or is unobstructed for the heating time constant.

In order to carry out the test, the operating conditions of the PTC were a flow rate of 4 litres per minute and a direct solar radiation of 865 W/m^2. The heating and cooling constants are reported in Table VII.

In Fig. 8, the red curve illustrates the exponential nature of the time constant of the PTC.

B. Thermal efficiency

The ASHRAE 93-1986(RA91) standard requires efficiency tests to be run for a period equal to one time constant or 5 min, whichever is larger.[33] Duration of all subsequent thermal efficiency tests was, therefore, set at 5 min to obtain feasible results. It is important to point out that the evaluation of the PTC system was done in the rage of 30 to 90 °C and a temperature ambient of 25 °C.

The thermal efficiency was evaluated by considering the temperature rise across the receiver $(\Delta T = T_i - T_a)$, where T_a is the ambient temperature and T_i is the inlet temperature. T_i

TABLE VII. The time constant for heating and cooling.

Time constant	
Cooling	Heating
63.5 s	45.5 s

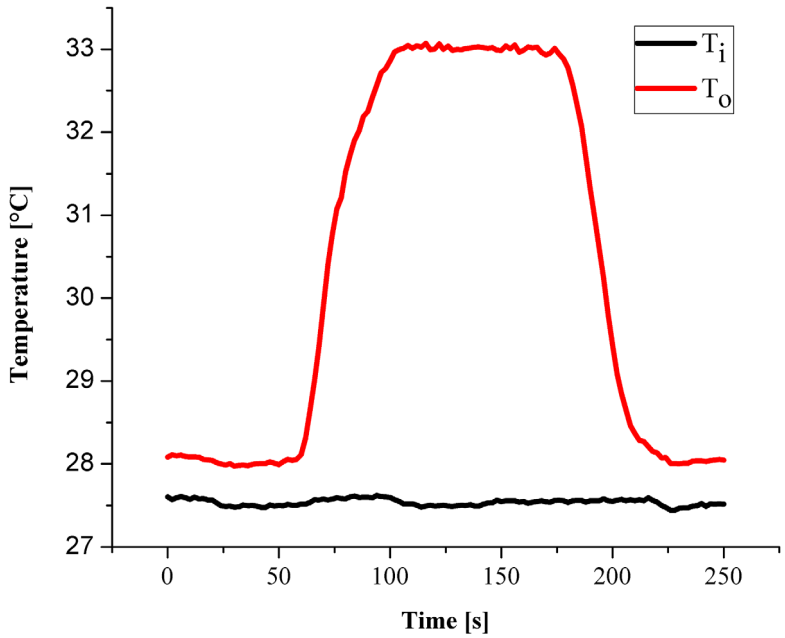

FIG. 8. Evaluation of the time constant.

was restricted to 92 °C to avoid the phase change of the water that is used as thermal fluid. First, Law thermal efficiency is given by[30,31]

$$\eta_I = F_R\left(\eta_o - \frac{U_L}{C_o}\left(\frac{\Delta T}{G_b}\right)\right), \tag{30}$$

which has the form of $y = b + mx$ that describes experimentally the heat removal factor F_R and the total heat loss coefficient U_L,[31] where the convective and radiative heat losses are included in this coefficient. This kind of linear model for the thermal efficiency is described by Duffie and Beckman[30] and Stine and Harrigan.[34] The efficiency curves for the PTC are shown in Fig. 9.

The values of the thermal efficiency η_I, the heat removal factor F_R, and the overall heat loss coefficient U_L are reported in Table VIII.

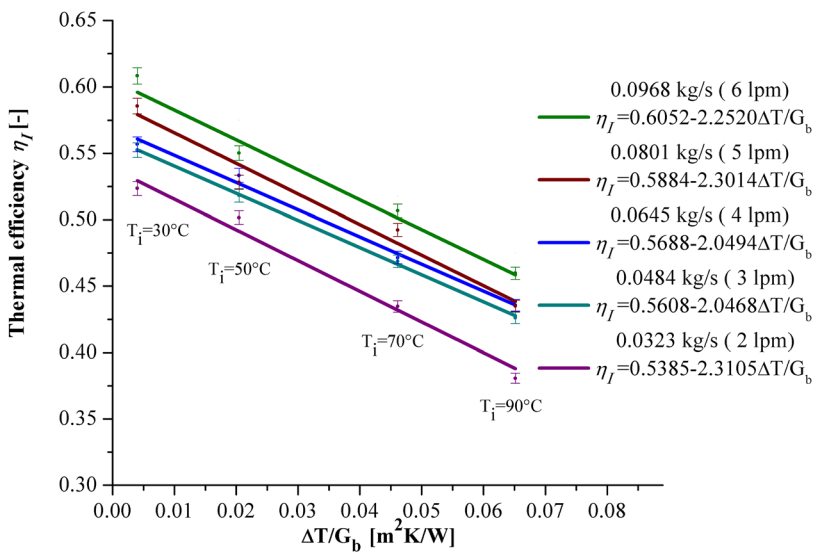

FIG. 9. Thermal efficiency data and best fit curve for the PTC.

TABLE VIII. Thermal performance of the PTC.

Parameters	Theoretical	Experimental
η_o (-)	0.60	0.60
η_I (-) at 4 lpm	$0.5574 - 2.3459(\Delta T/G_b)$	$0.5608 - 2.0468(\Delta T/G_b)$
C (-)	14.87	14.87
F_R (-)	0.929	0.935
U_L (W/m^{2}K)	37.55	32.56

C. Incidence angle modifier

The incidence angle modifier was evaluated according to the ASHRAE Standard 93-1986 (RA91) (section 8.3.4.2.2, Method 2). The value of K_θ is calculated by using Eq. (31), where the denominator represents the peak optical efficiency at normal incidence and the numerator shows the measured efficiency if the inlet fluid temperature is maintained equal to ambient temperature,[33]

$$K_\theta = \frac{\eta_I(T_i = T_a)}{F_R[\eta_o]_n}. \tag{31}$$

The incidence angle modifier was obtained experimentally according to the ASHRAE 93-1986 standard.[33] The regression analysis for the incidence angle modifier is described in Eq. (32),

$$K_\theta = 0.59834 + (0.0022)\,\theta_i - (1.1535 \times 10^{-4})\,\theta_i^2 - (4.46192 \times 10^{-8})\,\theta_i^3. \tag{32}$$

In Fig. 10, the curve shows the optical efficiency as a function of angle of incidence. The optical efficiency is 60% for $\theta_i = 0$, which is consistent with the theoretical results reported in Sec. III. Note that the optical efficiency decreases for large values of the angle of incidence because the PTC has a rim angle of 45° and the receiver is located at a long focal length. Thus, direct solar radiation is reflected and focused by the PTC, so it does not reach the receiver at large angles.

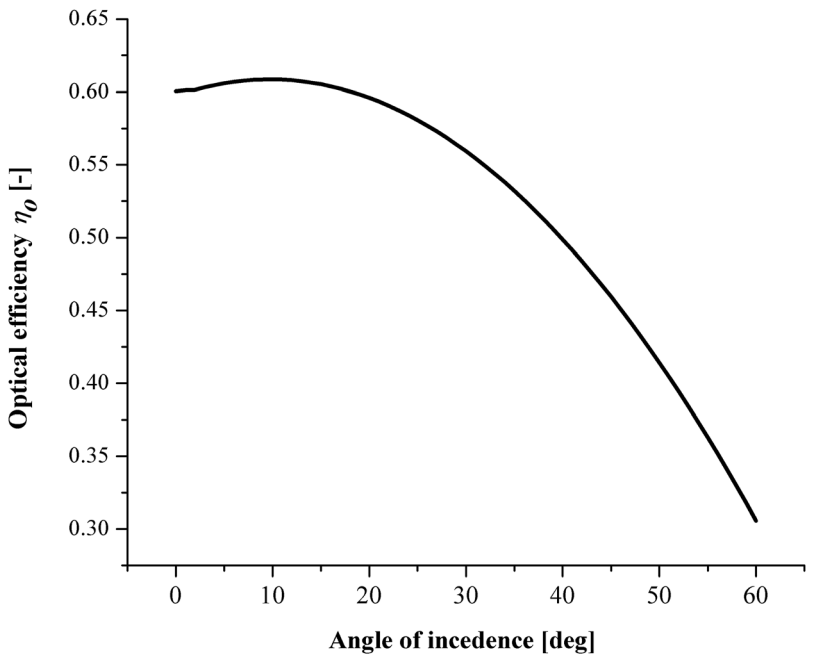

FIG. 10. Optical efficiency as a function of the incidence angle modifier at incidence angle θ.

TABLE IX. Initial cost of the solar PTC.

No.	Description	Cost ($USD)
1	7 aluminium ribs (material cost)	$120.00
2	5 aluminium structural tubes	$119.00
3	1 rectangular hollow section	$30.00
4	2 reflective foils	$110.00
5	1 absorber copper pipe	$35.00
6	4 structural edges	$57.00
7	3 absorber pipe supports	$45.00
8	7 CNC machining ribs	$110.00
9	Miscellaneous (insulations, screws, etc.)	$50.00
10	Support structure	$200.00
11	Tracking system (motor, pulleys, band)	$164.00
12	Labour for assembly (two workers)	$15.00
	Cost per collector	$1055.00
	Cost per m^2	$182.10

VI. COST ANALYSIS

The actual initial cost of the solar PTC system development in this research is laid out in Table IX. The material utilized for the constructions of the ribs and their CNC Machining are the most expensive parts in the manufacture of the PTC. For the manufacture of the PTC's ribs, we have taken into account the cost of an aluminium plate with dimensions of 1.22 × 3.05 m and 10 mm thick. It is possible to get 15 ribs with a rim angle of 45° from the aluminium plate. While it is necessary to include labour in the construction of the PTC, one must also take into consideration that a minimum degree of technical skill is required by workshop staff; therefore, the cost should not increase significantly.

The state of the art, up to 2005, regarding medium temperature solar collectors similar to the one developed in this paper can be found in Ref. 35. Their production costs range between 150 €/m^2 and 300 €/m^2. The prototype presented here has a cost around 145 €/m^2 as is reported in Table IX.

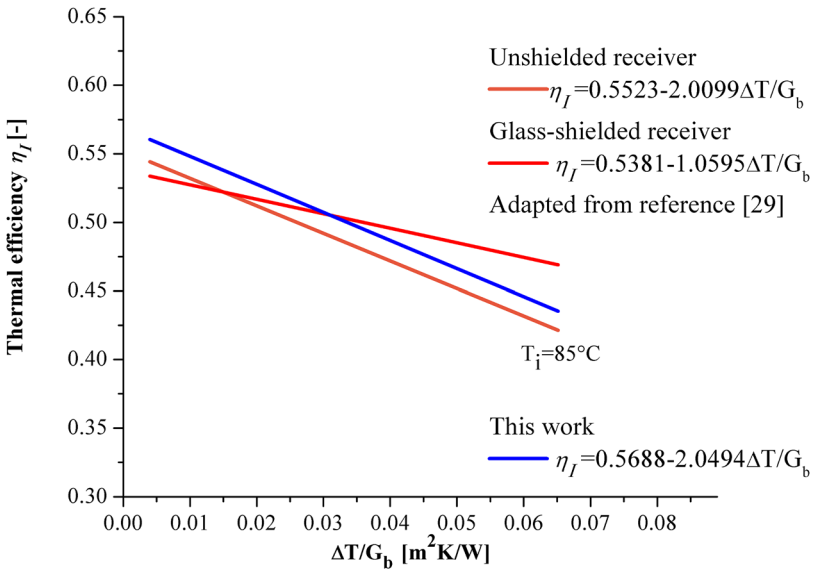

FIG. 11. Thermal efficiency. This work and Ref. 29.

It is important to point out that the estimated cost takes into account two unskilled assembly workers with a minimum wage for the particular case of Mexico.[36] This cost should be, therefore, adjusted for other countries accordingly.

VII. CONCLUSIONS

We present a novel design of a PTC with a rim angle of 45°, an aperture area close to 5.8 m^2, and a concentration ratio close to 15. The materials used in its construction and method of manufacture are inexpensive and do not require complex manufacturing techniques.

A finite element stress analysis was conducted to determine the mechanical behaviour of the PTC. The results show a maximum stress of 7.37 MPa for the lateral loads, which is lower than the permissible stress of aluminium that is 145 MPa. Therefore, the structural resistance of the collector is sufficient.

An optical error analysis was also carried out to evaluate the behaviour of the PTC. The optical efficiency of PTC is close to 60%. On the other hand, the intercept factor was estimated close to 67%. These results show that the mechanical design of the PTC provides an acceptable optical performance despite its simple construction.

A theoretical model for the thermal behaviour of the PTC was developed. The experimental results show that the model overestimates the losses in about 16% and underestimates the removal factor by about 2%. However, the overall results of the general model differ in 7% with respect to the experimental data. Despite the simplicity of the model, it provided an adequate estimation of the behaviour of the PTC.

The PTC was tested according to well known methodology based on to the ASHRAE 93-1986 (RA 91) standard. Tests were conducted to determine the collector time constant, thermal efficiency, collector acceptance angle, and incidence angle modifier. Peak efficiencies were evaluated and found to be close to 60%, showing an adequate heat removal factor collector. It can be observed in Fig. 9 that the slope is steep due to heat losses in the receiver. It is clear that the overall heat loss coefficient could be improved by using a glass-shielded receiver. However, considering the temperature range in which the PTC operates (between 70 and 110 °C), which is destined for soil disinfection we consider that augmenting the thermal availability by adding a glass tube is not necessary. Reference 29 reports that the instantaneous thermal efficiency for low temperature PTC's. As can be seen in Figure 11, the use of a glass shield does not translate into a significant increase in the efficiency for temperatures near 100 °C. It should also be mentioned that the use of glass-shielded receivers in developing countries like Mexico represents an increase in the associated costs given that such tubes are not fabricated locally and must be imported.

Given the geographical position of Mexico, solar heat for soil disinfestation by hot water and steam are very promising. However, large-scale implementation of solar thermal systems for this process requires the reduction of both investment costs and the financial risk. The PTC would benefit from further optimisation before commercial deployment.

ACKNOWLEDGMENTS

The authors wish to thank José de Jesús Quiñones Aguilar and Luis Gallardo Pérez for their technical assistance in the development of the experimental device and evaluation. We thank also Héctor Daniel Cortés González and Maximiliano González Valdez for their technical support in the network management. This work was supported by PAPIIT-UNAM under the Project IN113310.

[1]G. N. Kulkarni, S. B. Kedare, and S. Bandyopadhyay, "Determination of design space and optimization of solar water heating systems," Sol. Energy **81**, 958–968 (2007).
[2]G. N. Kulkarni, S. B. Kedare, and S. Bandyopadhyay, "Design of solar thermal systems utilizing pressurized hot water storage for industrial applications," Sol. Energy **82**, 686–699 (2008).
[3]J. M. Gordon and A. Rabl, "Design analysis and optimization of industrial process heat plants without storage," Sol. Energy **28**(6), 519–530 (1982).
[4]J. Atkins Martin, M. R. W. Walmsley, and A. S. Morrison, "Integration of solar thermal for improved energy efficiency in low-temperature-pinch industrial processes," Energy **35**, 1867–1873 (2010).

[5]A. Häberle, C. Zahler, F. Luginsland, and M. Berger, in *A Linear Concentrating Fresnel Collector for Process Heat Applications*, EUROSUN 2008, Lisbon, Portugal, 2008.
[6]A. Lokurlu, "Configurations of worldwide first solar cooling systems using parabolic trough collectors on locations in Turkey," in Proceedings of ISES World Congress 2007, Beijing, China, 2007.
[7]L. Ming, W. Liuling, Z. Xizheng, and L. Qing, "Study of a solar trough concentrating system for application of solar energy refrigeration," in *Proceedings of ISES World Congress 2007* (Springer, 2009), Vol. 3, pp. 556–560.
[8]S. A. Kalogirou and Y. Tripanagnostopoulos, "Industrial application of PV/T solar energy systems," Appl. Thermal Eng. **27**, 1259–1270 (2007).
[9]Renewable Energy in Industrial Applications, *An assessment of the 2050 potential*, United Nations Industrial Development Organization; available online at http://www.unido.org/fileadmin/user_media/Services/Energy_and_Climate_Change/Energy_Efficiency/Renewables_%20Industrial_%20Applications.pdf
[10]L. M. Murphy and E. Keneth, "Steam generation in line-focus solar collectors: A comparative assessment of thermal performance, operating stability, and cost issues," SERI/TR-1311, 1982.
[11]P. Hurtado and M. Kast, "Experimental study of direct in-situ generation of steam in a line focus solar collector," SERI, 1984.
[12]S. Kalogirou, S. Lloyd, J. Ward, and P. Eleftheriou, "Design and performance characteristics of a parabolic-trough solar-collector system," Appl. Energy **47**, 341–354 (1994).
[13]S. Kalogirou, "Parabolic trough collector system for low temperature steam generation design and performance characteristics," Appl. Energy **55**, 1–19 (1996).
[14]A. Valan Arasu and T. Sornakumar, "Performance characteristics of parabolic trough solar collector system for hot water generation," Int. Energy J. **7**, 137–145 (2006).
[15]A. Valan Arasu and T. Sornakumar, "Design, manufacture and testing of fiberglass reinforced parabola trough for parabolic trough solar collectors," Sol. Energy **81**, 1273–1279 (2007).
[16]N. Rosado Hau and M. A. Escalante Soberanis, "Efficiency of a parabolic trough collector as a water heater system in Yucatán, Mexico," J. Renewable Sustainable Energy **3**, 063108 (2011).
[17]F. Dabbene, P. Gay, and C. Tortia, "Modelling and control of steam soil disinfestation processes," Biosyst. Eng. **84**(3), 247–256 (2003).
[18]R. Berruto, P. Gay, P. Piccarolo, and C. Tortia, "Grey-box models for steam soil disinfestation simulation," Math. Comput. Simul. **65**(1–2), 191–200 (2004).
[19]P. Gay, P. Piccarolo, D. Ricauda Aimonino, and C. Tortia, "A high efficiency steam soil disinfestation system, Part I: Physical background and steam supply optimization," Biosyst. Eng. **107**(2), 74–85 (2010).
[20]P. Gay, P. Piccarolo, D. Ricauda Aimonino, and C. Tortia, "A high efficiency steam soil disinfestation system, Part II: Design and testing," Biosyst. Eng. **107**(3), 194–201 (2010).
[21]ALANOD Aluminium-Veredlung GmbH & Co. KG (2011), http://alanod.com/opencms/opencms/Eloxal/index.html.
[22]J. Ballestrín, S. Ulmer, A. Morales, A. Barnes, L. W. Langley, and M. Rodríguez, "Systematic error in the measurement of very high solar irradiance," Sol. Energy Mater. Sol. Cells **80**, 375–381 (2003).
[23]See www.algor.com for Algor simulation software, 2011.
[24]H. M. Güven and R. B. Bannerot, "Determination of error tolerances for the optical design of parabolic troughs for developing countries," Sol. Energy **36**(6), 535–550 (1986).
[25]H. M. Güven and R. B. Bannerot, "Derivation of universal error parameters for comprehensive optical analysis of parabolic troughs," J. Sol. Energy Eng. **108**, 275–281 (1986).
[26]H. M. Güven, F. Mistree, and R. B. Bannerot, "A conceptual basis for the design of parabolic troughs for different design environments," J. Sol. Energy Eng. **108**, 60–66 (1986).
[27]A. Rabl, *Active Solar Collectors and Their Applications* (Oxford University Press, USA, 1985).
[28]A. S. Metronor, Portable Coordinate Measurement Machine, Version 1.3, 2011. See www.metronor.com.
[29]M. J. Brooks, I. Mills, and T. M. Harms, "Design, construction and testing of a parabolic trough solar collector for a developing-country application," in Proceedings of the ISES Solar World Congress, Orlando, Florida, 6-12 August, 2005.
[30]J. Duffie and W. Beckman, *Solar Engineering of Thermal Processes*, 2nd ed. (Wiley-Interscience, USA, 1991).
[31]S. A. Kalogirou, *Solar Energy Engineering: Processes and Systems*, 1st ed. (Academic, USA, 2009).
[32]F. P. Incropera and D. P. DeWitt, *Fundamentals of Heat and Mass Transfer*, 5th ed. (Wiley, USA, 2002).
[33]ANSI/ASHRAE Standard 93, "Methods of testing to determine the thermal performance of solar collectors," 2003.
[34]W. B. Stine and R. W. Harrigan, *Solar Energy Fundamentals and Design with Computer Applications* (Wiley, USA, 1985).
[35]Werner Weiss, AEE INTEC, Matthias Rommel, Fraunhofer, "Solar heat for industrial processes, medium temperature collectors, state of the art within task 33/IV, subtask C," Solar Heating and Cooling Executive Committee of the International Energy Agency (IEA) (2005).
[36]See http://www.misalario.org/main/tu-salario/salario-minimo/mexico-salarios-minimos for minimum wage in Mexico (2012).